DTU Library

Unified approach to implicit and explicit solvent simulations of electrochemical reaction energetics

Gauthier, Joseph A.; Dickens, Colin F.; Heenen, Hendrik H.; Vijay, Sudarshan; Ringe, Stefan; Chan, Karen

Unified approach to implicit and explicit solvent simulations of electrochemical reaction energetics

Joseph A. Gauthier,[†,‡] Colin F. Dickens,[†,‡] Hendrik H. Heenen,[¶] Sudarshan Vijay,[¶] Stefan Ringe,[‡,†] and Karen Chan[*,¶]

†*SUNCAT Center for Interface Science and Catalysis, Department of Chemical Engineering, Stanford University, Stanford, California 94305, United States*

‡*SUNCAT Center for Interface Science and Catalysis, SLAC National Accelerator Laboratory, 2575 Sand Hill Road, Menlo Park, California 94025, United States*

¶*Department of Physics, Technical University of Denmark, DK-2800, Kgs. Lyngby, Denmark*

E-mail: kchan@fysik.dtu.dk

Abstract

One of the major open challenges in *ab initio* simulations of the electrochemical interface is the determination of electrochemical barriers under a constant driving force. Existing methods to do so include extrapolation techniques based on fully explicit treatments of the electrolyte, as well as implicit solvent models which allow for a continuous variation in electrolyte charge. Emerging hybrid continuum models have the potential to revolutionize the field, since they account for the electrolyte with little computational cost while retaining some explicit electrolyte, representing a "best of both worlds" method. In this work, we present a unified approach to determine reaction energetics from both fully explicit, implicit, and hybrid treatments of the electrolyte based on a new multi-capacitor model of the electrochemical interface. A given

electrode potential can be achieved by a variety of interfacial structures; a crucial insight from this work is that the *effective* surface charge gives a good proxy of the local potential, the true driving force of electrochemical processes. In contrast, we show that the traditionally considered work function gives rise to multi-valued functions depending on the simulation cell size. Furthermore, we show that the reaction energetics are largely insensitive to the countercharge distribution chosen in hybrid implicit/explicit models, which means that any of the myriad implicit electrolyte models can be equivalently applied. This work thus paves the way for the accurate treatment of *ab initio* reaction energetics of general surface electrochemical processes using both implicit and explicit electrolyte.

1   Introduction

Computational chemistry tools developed over the past several decades have allowed for an unprecedented level of mechanistic understanding in a wide variety of interface phenomena.[1–22] In particular, electrocatalysis has experienced a rapid expansion with the application of density functional theory (DFT). The computational hydrogen electrode model[23] has, in the past 15 years, enabled the determination of the thermochemistry of coupled ion-electron transfers using simple surface science calculations. For a number of applications, however, electrochemical reaction barriers,[24–37] electric field,[38–40] and pH effects,[41–43] are important, and all these elements require careful consideration of the electrolyte. Several methods have since been developed to model the electrochemical interface in *ab initio* simulations. Fully explicit simulations of the electrolyte[44–46] have been developed, and in parallel, different implicit solvation methods have been implemented in a variety of commonly used DFT codes.[17,47–64]

Each of these techniques comes with their own advantages and shortcomings. Fully explicit techniques give atomistic insight to the effects of solvation and the effect of electric field on reaction energetics.[13,40,44] However, they frequently rely on expensive electrolyte sampling

methods,[11,65–67] and furthermore suffer from issues related to band misalignment,[68] stemming from the well known failure of GGA-DFT under-predicting bandgaps.[69] Continuum methods present thermodynamic averages of solvation and therefore do not rely on expensive sampling techniques. They do however come with a variety of challenges[70] primarily from the marrying of the classical treatment of solvation with the atomistic treatment of the surface. Most importantly, continuum methods intrinsically cannot reproduce the chemical interaction of the surface with ions, since the charge is necessarily smeared over the entire electrode surface. Solvation energies for these methods have primarily been fit to molecular solutes, since that is the source of most experimental reference data.[47,54,56,71] Little work has been done to benchmark these energies on extended surfaces, where hydrogen bonding has been shown to be important.[25,72–74] For these reasons, hybrid approaches, including both some explicit electrolyte molecules and continuum solvation, are receiving a growing amount of attention, especially in applications where atomistic level details are significant.[75,76]
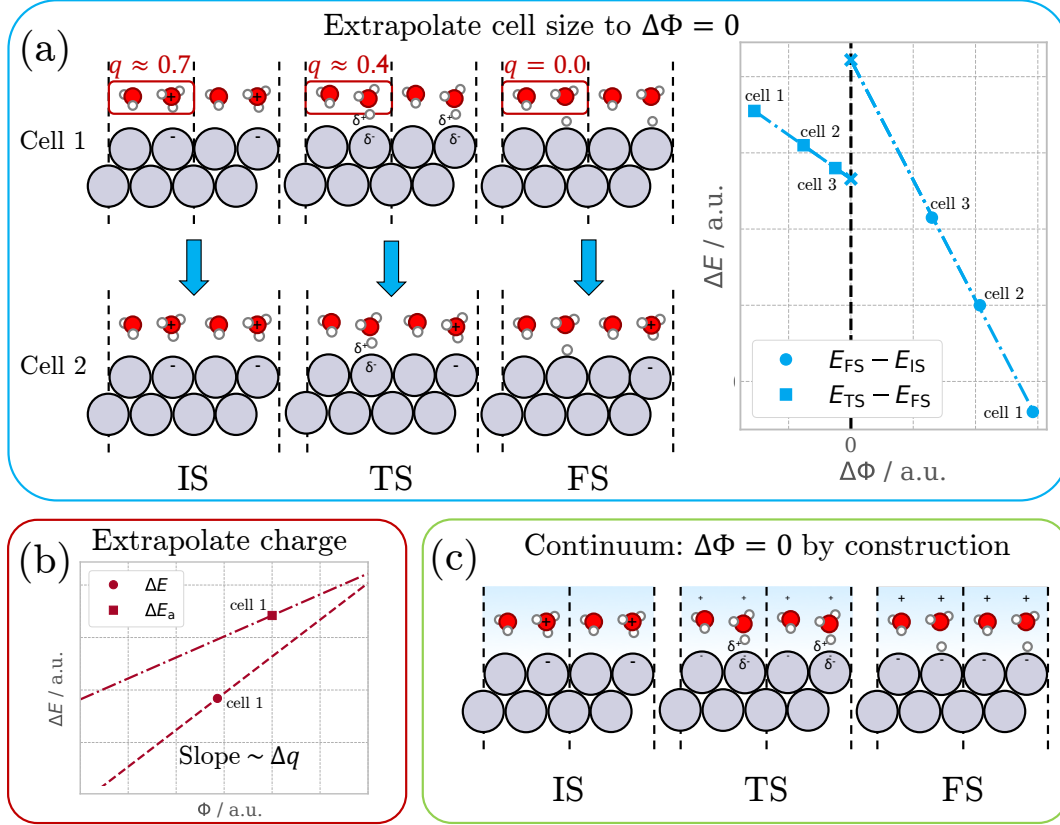
Figure 1: Schematic of three current state of the art methods for calculating reaction energetics at constant driving force. (a) Schematic of cell extrapolation for two cell sizes, and illustration of charge partitioning (e.g. Bader) to determine the charge of the ion at the interface for charge extrapolation. (b) Charge extrapolation technique, with charges determined by partitioning as illustrated in (a). (c) Continuum charging, which exchanges electrons with an external reservoir to achieve constant work function. Counter charge is placed in the electrolyte to retain overall charge neutrality.

Real electrochemical systems operate at a constant applied electrode potential, and so there has been an effort to develop computational models that allow for simulations at constant potential. This is particularly challenging, since the work function, which defines the potential in *ab initio* simulations, changes across the reaction coordinate due the use of finite simulation cell sizes. Figure 1 illustrates three classes of techniques used currently to solve the problem of changing work function across the reaction coordinate during charge transfer reaction events. Cell extrapolation, illustrated in Figure 1(a), relies on systematically increasing the size of the simulation cell in order to more closely approximate the infinite cell size limit. This approach can be quite expensive computationally, owing to the roughly cubic scaling of DFT with system size.[77] Charge extrapolation, illustrated in Figure 1(b), instead utilizes a mean-field (i.e. capacitor) approximation of the interface to predict the slope of the energy as a function of potential, which is proportional to the change in charge between states. The primary difficulty with this method is identifying the charge in each state. Previous work has shown that the charge resulting from charge partitioning schemes (e.g. Bader[78–80]) can accurately reproduce the results from cell extrapolation,[45,46] but it is not clear how to partition charge for field-sensitive chemical steps. Finally, continuum charging methods, shown in Figure 1(c), allows for continuous variation in charge, leading to the possibility of the work function being constant between states at little additional computational cost.[75]

In the present work, we present a unified approach to determining reaction energetics for general hybrid or fully explicit electrolyte models of the interface. This framework is based on 1) a *multi-capacitor* model of the various components of an electrochemical interface in atomistic DFT simulations 2) the idea that an *effective surface charge density* is the appropriate descriptor for the electrochemical driving force of electrochemical reactions, as opposed to the generally applied work function. The latter is essentially a reformulation of the Frumkin correction to reaction kinetics,[81,82] which emphasizes that the *local* potential drop at the interface between the metal and reaction plane potential is the driving force

for electrochemical reactions. What we assert here is that this local potential drop is best approximated by an *effective* surface charge density. In contrast, the traditional use of work function as a descriptor of the driving force leads to multi-valued, cell-size dependent functions of reaction energetics in hybrid implicit/explicit "constant-potential" simulations. We further show that, within our framework, the reaction energetics are essentially insensitive to the distribution of the continuum countercharge, which means that any of the myriad of existing implicit electrolyte models can be equivalently applied. By using the effective surface charge as the descriptor for the driving force, we importantly avoid the need to parameterize the continuum model to accurately predict capacitances. The calculated capacitances also vary significantly upon the addition of explicit water layer(s) or at high coverages of some adsorbates, which renders parametrizations to bare surfaces obsolete. The energetics obtained through our method as a function of surface charge can be related to experimental activities through a coupled double-layer charging kinetic model, where diffuse layer effects can be accounted for,[83] essentially removing the need to predict capacitance. The framework we present here solves the observed cell-size dependence in hybrid explicit-implicit solvation constant potential simulations, and therefore represents a major step forward in the computational modeling of electrochemical reaction energetics.

2 Theoretical Methods and Models

This work uses the Vienna ab-initio Software Package[84–86] in conjunction with VASPsol,[56,57] as well as QUANTUM-ESPRESSO[87] (QE) in conjunction with the Environ[47] solvation module. Using VASP, core electrons were modeled with projector augmented wave pseudopotentials; using QE, core electrons were modeled using GBRV ultrasoft pseudpotentials.[88] In both DFT codes, valence electrons were expanded as plane-waves up to a kinetic energy cutoff of 500 eV. Exchange and correlation interactions were accounted for using the RPBE functional[89] in both codes. When optimizing bulk platinum to determine the appropriate

lattice constant, the Brillouin zone was sampled with a 12 x 12 x 12 γ-centered Monkhorst-Pack[90] k-point mesh. The optimized Pt lattice constant was determined to be 3.990 Å in VASP, and the optimized Cu lattice constant was found to be 3.6 Å in QE.

Geometries were considered optimized when the maximum force on any unconstrained atom in the system was below 0.03 eV $\mathring{A}^{-1}$. For each electronic self-consistent field calculation, the density was considered to have converged when the total energy changed by less than 10^{-4} eV between steps. Separation between periodic images was set to be 8 Å. Using our previously published methodology,[91] we have corrected the constant charge reaction energetics by $q\Delta\Phi_{vac}$, where q is the (implicit) system charge and Φ_{vac} is the potential of the electrolyte region. This term accounts for the shift in potential necessary with VASPsol and eliminates cell height dependence of the energetics.[91] To avoid possible spurious dipole interactions, our simulation cells are symmetric along the direction normal to the surface.

VASPsol and Environ both treat the electrolyte at the electrochemical interface as a polarizable continuum. VASPsol places counter-charge via the linearized Poisson-Boltzmann equation, while Environ allows for a variety of countercharge placement models. In this work, except when stated otherwise, we use VASPsol, which places countercharge by solving the linearized Poisson-Boltmzann equation. Within this model we choose a Debye length of 3.0 Å, corresponding to a bulk ion concentration of 1.0 M. We set the effective surface tension to zero to avoid numerical instabilities, as reported in a recent perspective.[70] When Environ is used, we use the planar countercharge, modified Poisson-Boltzmann, and linearized modified Poisson-Boltzmann countercharge placement models. We use the standard g03-SCCS solvation parameters.[47] Details regarding the implementation of these solvation models can be found in their documentation.[47,56,57]

3   Results and Discussion

We consider different kinds of charged interfacial systems as visualized in Figure 2: adsorbed partially negatively charged CO_2, explicitly modeled hydronium cations and a continuum representation of electrolyte counter ions at the outer Helmholtz plane. All of these systems give rise to a separation of negative and positive charge, which can be effectively envisioned as local capacitors. In the case of explicit (e.g. proton) charge, the effective capacitor charge is just that of the proton itself, which is slightly less than unity.[92] In the case of CO_2, partial charge, corresponding to the electrosorption valency, is transferred during the adsorption process which leads to the creation of a strong dipole moment.[93–95]
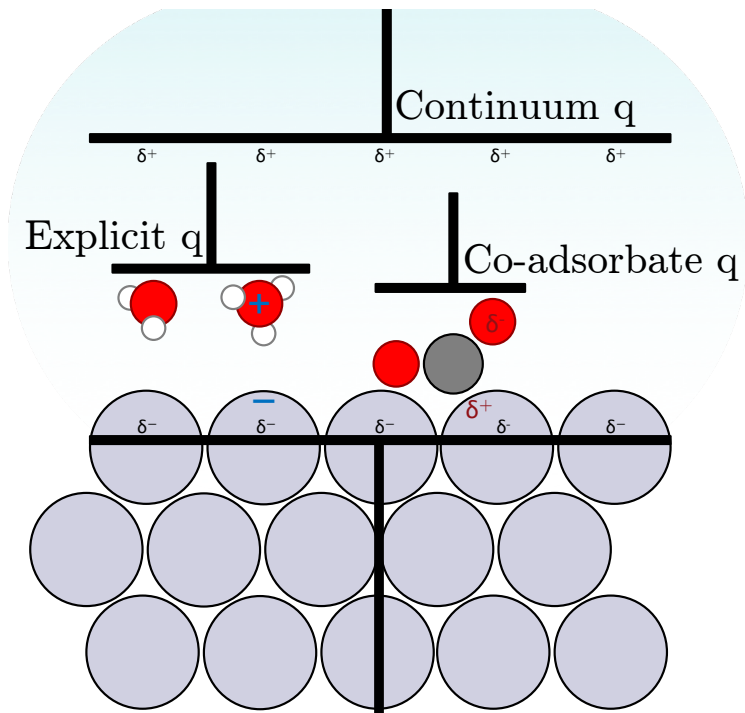
Figure 2: Illustration of three different potential dependent processes that can be effectively modeled by adiabatic DFT approaches: CO_2 adsorption, charge transfer reactions (e.g. $(H^+ + e^-) + * \rightarrow H*$), and continuum charging/counter-charging.

The *local* potential drop at the interface, between the metal potential and the solution potential at the reaction plane, is the driving force for electrochemical reactions. This is the essential idea behind the Frumkin diffuse layer correction to reaction kinetics.[81,82] As we

show below, this local potential drop is better approximated by the total effective surface charge than the overall work function. This concept is illustrated in Figure 3, where the potential drop across the electrochemical interface is illustrated. Here the work function is given by the potential difference between the metal surface and the bulk electrolyte level, $\Phi_M - \Phi_{\cancel{vac}bulk}$. However, the driving force for charge transfer is instead described by $\Phi_M - \Phi_{RP}$, since the transition state lies in this region.
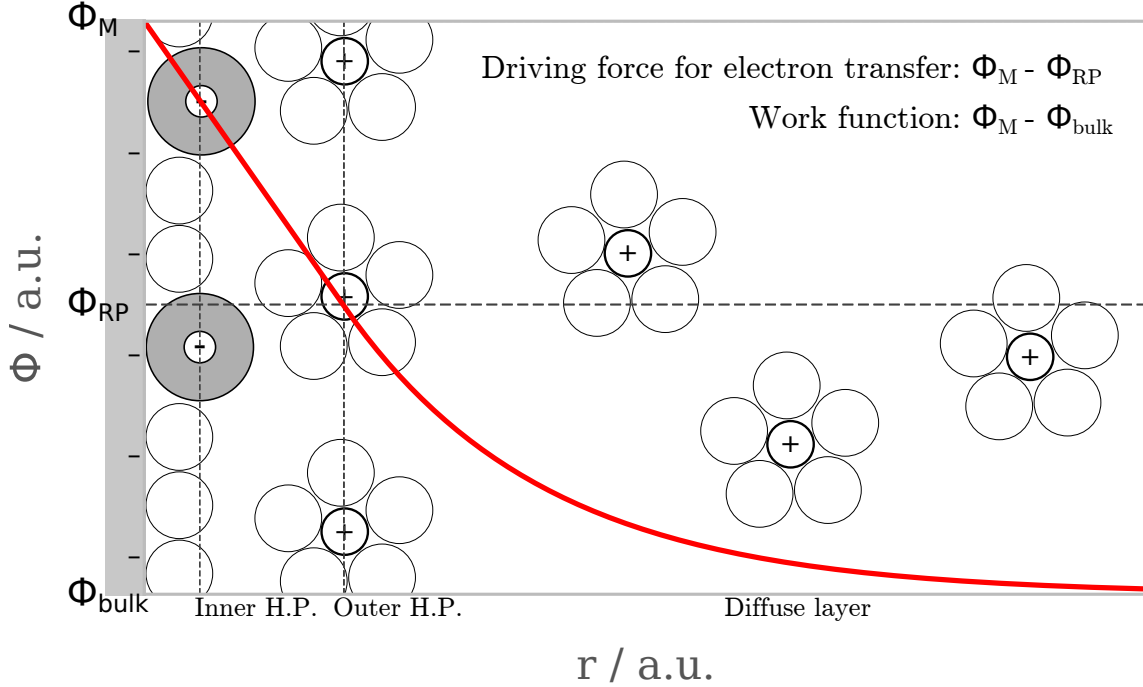

Figure 3: Illustration of the potential drop across the electrochemical interface. Here the surface (drawn as the left side of the plot), is covered by charge neutral solvent molecules (solid white circles) and anions (dark gray circles). Solvated cations form a Helmholtz like layer demarcating the outer Helmholtz plane, followed by the diffuse layer. The linear potential drop between the surface and the reaction plane gives the driving force for electron transfer ($\Phi_M - \Phi_{RP}$), while the work function is given by potential drop between the surface and the bulk electrolyte potential ($\Phi_M - \Phi_{bulk}$).

In what follows, we derive a generic multi-capacitor model of the electrochemical interface,[17,45,46,96–99] starting with the simple case of an interface with one charging component. We use this model to develop expressions relating electrochemical reaction energetics to both excess surface charge density, and the work function. We then show the "effective" surface

charge density to be the appropriate descriptor of the driving force, since it reflects the local potential drop. We demonstrate that, using the work function (a measure of the applied potential) as the descriptor, the reaction energetics are not uniquely defined. We then develop a framework to calculate electrochemical reaction energetics in general.

3.1 General Multi-Capacitor Model of the Electrochemical Interface

3.1.1 Energy of the Charged Interface

We first review the energy of the charged interface undergoing only one charging process. We can expand the energy as a Taylor expansion about a hypothetical zero interfacial charge $q = 0$, corresponding to a work function Φ_0, as has been done in previous works.[17,96–99]

$$E = E^0 + \frac{\partial E}{\partial q}\bigg|_{q=0} q + \frac{1}{2}\frac{\partial^2 E}{\partial q^2}\bigg|_{q=0} q^2 + \mathcal{O}(q^3) \quad . \tag{1}$$

Here $E^0 = E|_{q=0}$ is the energy of all *non-electrostatic* (i.e. chemical) components of the system at the hypothetical $q = 0$ case, which corresponds to the case of zero partial charges in Figure 2. This case is exemplified by, for instance, a hypothetical neutral H_3O molecule solvated above a metal slab (as opposed to a positively charged H_3O molecule solvated above a negatively charged metal slab), or a hypothetical adsorbed CO_2 molecule with no dipole moment.

By definition,

$$\frac{\partial E}{\partial q}\bigg|_{q=0} = \Phi_0 \tag{2}$$

where Φ_0 is the work function at zero charge, referenced to the bulk electrolyte potential. We further assume here that we have a constant capacitance C, which we find to be valid

in small potential ranges, as discussed later in this work:

$$\frac{\partial}{\partial q}\left(\frac{\partial E}{\partial q}\right) = \frac{\partial \Phi}{\partial q} = \frac{1}{C} \quad , \tag{3}$$

such that (1) becomes.

$$E = E^0 + q\Phi_0 + \frac{q^2}{2C} \quad . \tag{4}$$

We now use the capacitor equation $q = C(\Phi - \Phi_0)$ to write (1) in terms of Φ

$$E = E^0 + C(\Phi - \Phi_0)\Phi_0 + \frac{C(\Phi - \Phi_0)^2}{2} \quad . \tag{5}$$

Or without reference to the capacitance,

$$E = E^0 + q\Phi_0 + \frac{q(\Phi - \Phi_0)}{2} \quad . \tag{6}$$

As an example, we show the energetics of Pt (111) as a function of both excess surface charge q as well as the work function Φ in Figure 4. Here the surface was charged using the linearized-Poisson Boltzmann equation to place countercharge. The slight deviations from the model in panel (b) results from the capacitance being non-linear far from the potential of zero charge. From a linear fit of the surface charge as a function of potential, we calculate a surface capacitance C of 25 $\mu F\,cm^{-2}$, and a work function of zero charge Φ_0 of 5.4 eV.
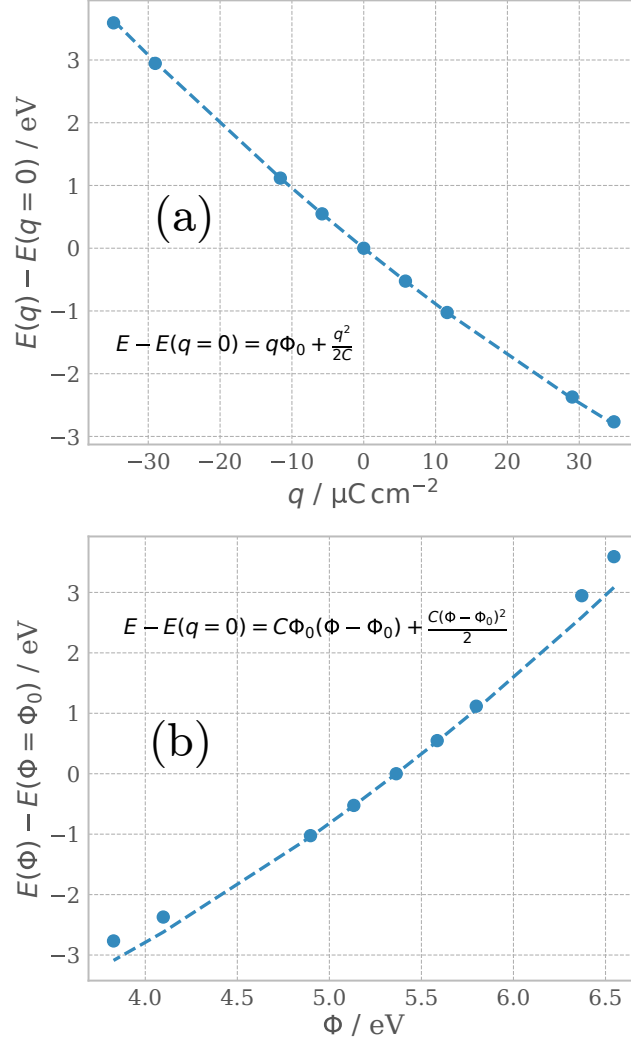
Figure 4: Energetics of Pt(111) as a function (a) excess implicit surface charge q, where dashed lines correspond to Eq. (4), and (b) work function Φ, where dashed lines correspond to Eq. (6). Panel (b) shows slight deviations far from the work function of zero charge (≈ 5.4 eV in this picture) due to the nonlinear capacitance behavior far from the PZC.

3.1.2 Reaction Energetics: Only One Charging Component

We now consider the energetics of an interfacial charge-transfer reaction, i.e. charging process of any of the envisioned capacitors in Figure 2. Considering an infinitely extended system, the a single reaction event such as adsorption or proton-electron transfer does not change the work function of the metal electrode. In a typically used finite unit cell setup, however, the these processes critically changes the electrode work function. As before, the hypothetical $q = 0$ state is one such that there is no charge separation; for example, a hypothetical neutral hydronium molecule solvated above an uncharged metal slab, or a hypothetical CO_2 molecule adsorbed with no dipole moment. We can therefore assume that Φ_0 does not change between the states considered. We find that in practice, the capacitance varies by only a very small amount for a large change in surface coverage, changing from 12.6 $\mu F\,cm^{-2}$ for a clean Pt (111) surface to 10.1 $\mu F\,cm^{-2}$ with CO_2 adsorbed in a 2x2 supercell, the smallest cell size considered here (and hence the highest coverage). This capacitance drop reduces to just 0.1 $\mu F\,cm^{-2}$ in a 4x4 supercell, as we reported in a recent work.[91] We therefore assume that the capacitance between different states along a reaction pathway does not vary. While, in this work, this assumption has been found to be robust for a variety of adsorption and charge transfer reactions in an aqueous electrolyte, it is not entirely general. For instance, linear solvation models, as are used in this work, have been shown to underestimate interfacial capacitances on metal surfaces,[100] which may make the observed nearly constant capacitance a better approximation than for other solvation models. Ionic liquid structures near metal surfaces can also undergo potential-induced phase transitions which give rise to substantial changes to the capacitance.[101,102] [1]

Under these assumptions, from Eq. (4), we have the change in energy from state 1 to

---

[1]We note that, as we discuss in section 3.1 and 3.2 below, the capacitnance C_{impl} corresponding to the second charging component in a given model system (whether implicit models or co-adsorbates) does not enter into the energetics at all when surface charge density is considered as the descriptor for the driving force for an electrochemical process (cf. Eq 15.)

state 2 (denoted as subscript 1 and 2, respectively) as

$$\Delta E = \Delta E_0 + (q_2 - q_1)\Phi_0 + \frac{q_2^2 - q_1^2}{2C} \tag{7}$$

$$= \Delta E_0 + (q_2 - q_1)\left(\frac{\overline{q}}{A\widetilde{C}} + \Phi_0\right) \quad, \tag{8}$$

where we have defined the average charge $\overline{q} = \frac{1}{2}(q_1 + q_2)$ and introduced the surface area normalized capacitance, $\widetilde{C} = C/A$. Eq. (8) can also be written as a function of work function via $q = C(\Phi - \Phi_0)$,

$$\Delta E = \Delta E_0 + (q_2 - q_1)\overline{\Phi} = \Delta E_0 + \frac{C}{2}(\Phi_2^2 - \Phi_1^2) \quad, \tag{9}$$

where we have similarly defined $\overline{\Phi} = \frac{1}{2}(\Phi_1 + \Phi_2)$.

In the limit of an infinitely sized simulation cell where $A \to \infty$, the corresponding effect of the dipole shift on the potential and surface charge density is infinitesimal, i.e. $\Phi_1 \to \Phi_2$ and $q_1/A \to q_2/A$. However $q_1 \nrightarrow q_2$ since even in the infinite cell size limit, there is still finite charge transfer across the reaction coordinate. In the infinite cell size limit, we therefore have $\overline{\Phi} \to \Phi$ and $\overline{q} \to q$. In the supporting information (SI) Note 1, we show that the change in energy as a function of the average work function is equivalent to the cell-extrapolated (i.e. infinite cell size, constant potential) energetics detailed in Ref. 44

The effective charge transferred $q_2 - q_1$ can be determined by evaluating the reaction energetics at multiple finite cell sizes and then fitting either Eq. 8 or Eq. 9, i.e.

$$q_2 - q_1 = \frac{\partial \Delta E}{\partial \overline{\Phi}} = \frac{\partial \Delta E}{\partial \left(\frac{\overline{q}}{A\widetilde{C}}\right)} \quad. \tag{10}$$

In the case of a simple proton-electron transfer, it has been shown in previous work that $q_2 - q_1$ can usually be determined through the Bader[78–80] charge of the slab and adsorbates (i.e. the charge extrapolation model).[45,46]

We note here that in the case of an adsorption reaction event, the calculated effective

14

charge transferred $q_2 - q_1$ is the difference in physical charge separation at the interface between the two states, giving rise to the corresponding capacitance of the given process. This is not necessarily Faradaic charge transferred across the reaction. For example, the process of adsorbing a CO_2 on the surface creates a substantial dipole moment, which has an associated charge separation despite no Faradaic charge being transferred in the reaction event. In the example of CO_2 adsorption, $q_2 - q_1$ yields the effective surface charge associated with a polarized CO2 molecule. For the Volmer reaction, $q_2 - q_1$ yields the effective surface charge transferred with the proton transfer from the Helmholtz plane to the surface. Naturally, $q_2 - q_1$ could also represent the charge difference via continuum charging of any surface composition.

To illustrate these charging behaviors, we have plotted the energetics of a simple proton-electron transfer process (Volmer, i.e. $(H^+ + e^-) + * \rightarrow H*$) and CO_2 adsorption on Pt (111) as a function of the work function Φ in Figure 5. In this picture, no continuum solvation or charging is used; the different scatter points are achieved by changing the coverage of protons and CO_2, respectively by changing the unit cell size.
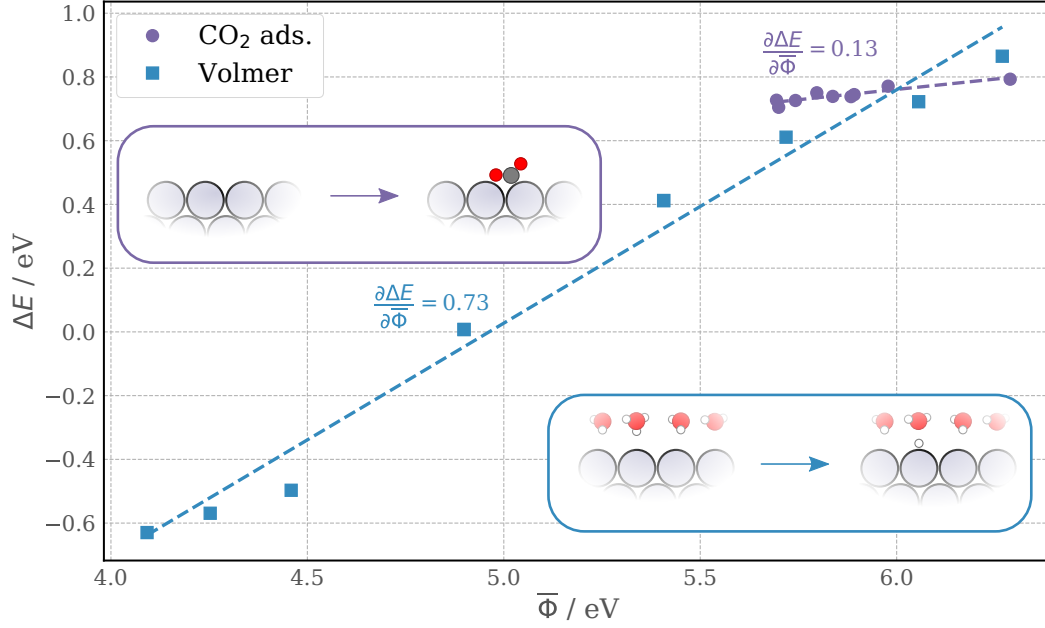
Figure 5: Energy as a function of average work function, $\overline{\Phi} = \frac{1}{2}(\Phi_{IS} + \Phi_{FS})$ for CO_2 adsorption on Pt (111) and the Volmer reaction (i.e. $(H^+ + e^-) + * \rightarrow H*$) on Pt (111), with no continuum solvation. The different scatter points are calculated by changing the coverage of CO_2 and protons by, for instance, changing the cell size. Here the x-axis is the average work function between the initial and final state, and so the slopes in this plot correspond to a fit of q_{eff} as given in Eq. (10).

3.1.3 Reaction Energetics: Two Charging Components

We now consider the case of a reaction energy evaluated where a second charging component is present and constant throughout the reaction pathway. For example, a Volmer reaction event where a constant continuum charge q_{impl} or an additional co-adsorbate with a significant dipole moment is added to the two states considered. As we illustrated in a previous work,[91] the energetics obtained with such a constant charge setup, when considered as a function of $\overline{\Phi}$ between the states considered, are equivalent to the grand canonical energy difference at constant potential. The latter method of charging the interface to achieve constant potential has been applied to a wide variety of surface electrochemical reactions,[75,103–105] since it allows a simple way to probe energetics across a large range of work functions.

For a general system with both implicit and explicit charging, we apply Eq. (7) to expand the energy about $q_{\mathrm{impl}} = 0$, giving a total reaction energy as the sum of contributions from both explicit and implicit charging,[2]

$$\Delta E = \Delta E_{\mathrm{expl}} + \Delta E_{\mathrm{impl}} \tag{11}$$

$$= \Delta E_{\mathrm{expl}} + q_{\mathrm{impl},2}\Phi_2 - q_{\mathrm{impl},1}\Phi_1 + \frac{q_{\mathrm{impl},2}^2 - q_{\mathrm{impl},1}^2}{2C_{\mathrm{impl}}} \quad . \tag{12}$$

where ΔE_{expl}, the component arising from explicit charging, is given by Eq. (8). We introduced the capacitance associated with charging the interface with a continuum charge, C_{impl} and note that it need not equal the capacitance associated with charging the interface via other methods.

In the constant charge setup, the continuum charge q_{impl} is constant between the states considered (e.g. initial and final) i.e. $q_{\mathrm{impl},1} = q_{\mathrm{impl},2} = q_{\mathrm{impl}}$. The reaction energy then

---

[2]We note here that the coupling term in this Taylor expansion has been incorporated into the expression for Φ_i, i.e. $\Phi_i = \Phi_0 + \dfrac{q_{\mathrm{expl},i}}{C_{\mathrm{expl}}}$

reduces to

$$\Delta E = \Delta E_{\text{expl}} + q_{\text{impl}} \left(\Phi_2 - \Phi_1 \right) \tag{13}$$

$$= \Delta E_0 + (q_2 - q_1) \left(\frac{\overline{q}_{\text{expl}}}{C_{\text{expl}}} + \Phi_0 \right) + q_{\text{impl}} \left(\frac{q_2 - q_1}{C_{\text{expl}}} \right) \tag{14}$$

$$= \Delta E_0 + \frac{q_2 - q_1}{\widetilde{C}_{\text{expl}}} \left(\frac{\overline{q}_{\text{expl}} + q_{\text{impl}}}{A} + \widetilde{C}_{\text{expl}} \Phi_0 \right) \quad . \tag{15}$$

3.2 Effective Surface Charge Density as the Appropriate Descriptor of Driving Force

As we noted previously, two independent charging components need not have identical associated capacitances. Here, we demonstrate that unequal capacitances lead to the average work function not uniquely defining the energetics, and that the surface charge density is a better descriptor of the local driving force.

To write Eq. (15) in terms of potential, we first write

$$\frac{\overline{q}_{\text{expl}}}{C_{\text{expl}}} + \Phi_0 = \frac{\Phi_2 - \Phi_0 + \Phi_1 - \Phi_0}{2} + \Phi_0 = \overline{\Phi}_{\text{expl}} \quad , \tag{16}$$

and note that

$$q_{\text{impl}} = C_{\text{impl}}(\Phi_{\text{impl},2} - \Phi_2) = C_{\text{impl}}(\Phi_{\text{impl},1} - \Phi_1) \tag{17}$$

$$= C_{\text{impl}} \left(\frac{\Phi_{\text{impl},2} + \Phi_{\text{impl},1}}{2} - \frac{\Phi_2 + \Phi_1}{2} \right) \tag{18}$$

$$= C_{\text{impl}}(\overline{\Phi}_{\text{impl}} - \overline{\Phi}_{\text{expl}}) \quad . \tag{19}$$

Inserting this expression into Eq. (15), we arrive at the reaction energy as a function of potential,

$$\Delta E = \Delta E_0 + (q_2 - q_1) \left[\overline{\Phi}_{\text{expl}} + \frac{C_{\text{impl}}}{C_{\text{expl}}} (\overline{\Phi}_{\text{impl}} - \overline{\Phi}_{\text{expl}}) \right] \tag{20}$$

Equation (20) demonstrates that, if the ratio $C_{\text{impl}}/C_{\text{expl}}$ is non-unity, the average po-

tential does not uniquely describe the reaction energy. In other words, for a given potential, the reaction energy can take on multiple values depending on the charging method used to achieve that potential.

We demonstrate this finding with two examples: the Volmer reaction, and CO_2 adsorption shown in Figure 6. We systematically modify the potential by varying both the explicit charge (i.e. changing the cell size and proton/CO_2 coverage) as well as with continuum charge (i.e. using "constant-potential" implicit solvation methods). A third example, CO_2 adsorption with varying co-adsorbates, can be found in SI Note 2. Figure 6 (a) shows that the reaction energy for Volmer is not uniquely determined by the potential, because the capacitance associated with explicit charging ($C_{\mathrm{expl}} \approx 20\mu\mathrm{F\,cm^{-2}}$) and continuum charging ($C_{\mathrm{impl}} \approx 9\mu\mathrm{F\,cm^{-2}}$) are significantly different. We note that these capacitances are fit via $q = C(\Phi - \Phi_0)$, as described in the first section. In contrast, Figure 6 (a) shows the reaction energy associated with CO_2 adsorption as a function of potential, similarly modifying the potential both with explicit (i.e. CO_2 coverage) and continuum charging. The agreement between continuum and explicit charging in this picture is much better, since the capacitance for each associated process is approximately identical ($C_{\mathrm{expl}} \approx 12\mu\mathrm{F\,cm^{-2}}$, $C_{\mathrm{impl}} \approx 14\mu\mathrm{F\,cm^{-2}}$).
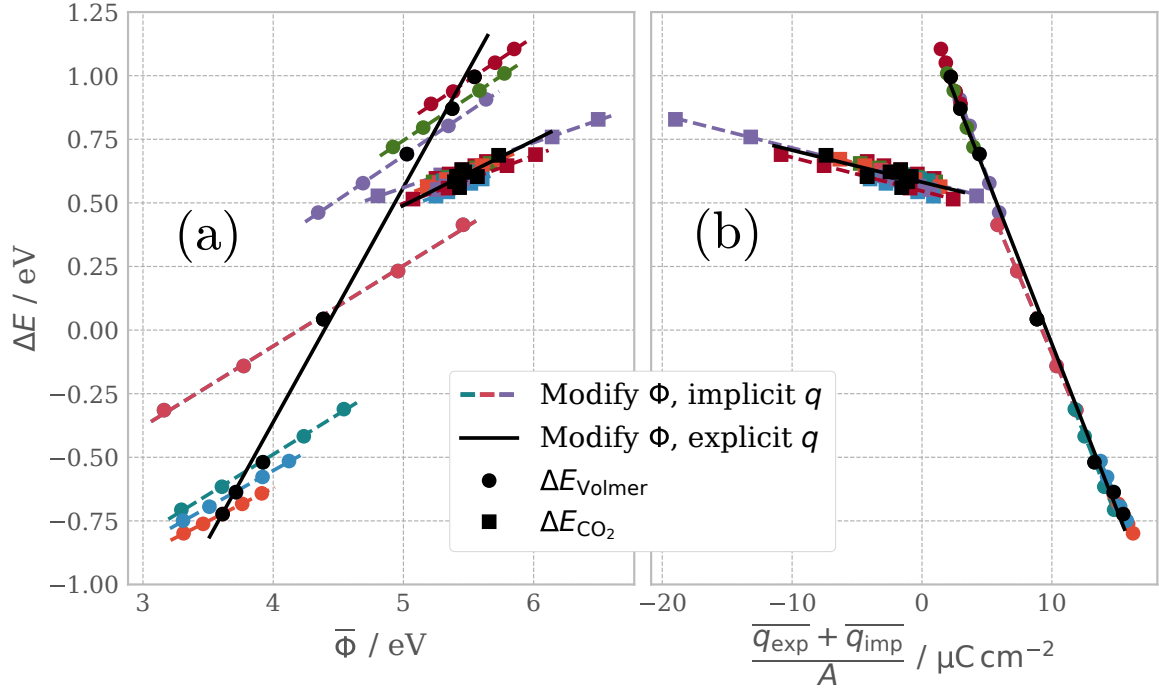
Figure 6: Reaction energetics of CO_2 adsorption and the Volmer reaction as a function of (a) the average work function (i.e. the grand canonical constant potential reaction energy), corresponding to the potential as the descriptor for the driving force, as in Eq. (9). Panel (b) shows the same data set with the driving force given instead by the effective surface charge, $\frac{1}{A}(\overline{q}_{expl} + q_{impl})$, as expressed in Eq. (15).

Figure 6 (b) then shows the energetics as a function of the effective surface charge density, corresponding to Eq. (15). Here it can be seen that regardless of the variation in capacitance, the energetics are uniquely defined. Since the capacitance for the two processes in the case of CO_2 adsorption are similar, the level of error reduction is minimal. However, for the case of the Volmer reaction, the clearly non-collinear lines collapse onto a single line.

This result suggests that even for the previously established "constant-potential" hybrid implicit solvation methods, if the capacitances associated with the explicit and implicit charging are not equal, there is a cell size dependence in the computed energetics. This is because these methods do not achieve constant local potential; rather, they are constant bulk potential, and in these systems the work function acts as a poor descriptor of the local potential, which is better described by the *effective* surface charge.

In principle, in the special case where the capacitance of all components are equal, then the work function again would provide single-valued functions of energy (see SI Note 3). However, this would require adjustment of the solvation parameters for each individual system to match the capacitances, which would then lead to inconsistent solvation energies amongst the systems considered.

We note that although we chose subscripts *expl* and *impl* in our derivation of the model for energetics with two charging components, the model is not specific to explicit and implicit charging. An example of this model working for a case with no implicit charging is illustrated in SI Note 2, where we show the binding energy of CO_2 (charging component 1) with various co-adsorbed ions (charging component 2). In this case, there is a charge associated with CO_2 denoted q_{CO_2} and a charge associated with the co-adsorbate denoted q_{ion}, which replaces subscripts *exp* and *imp* in our derivation.

3.3   Insensitivity of the Driving Force to Water Structure

An additional challenge associated with describing the reaction energetics as a function of work function arises for the case of explicit solvation. For a given charge state, the work

function of a surface can vary dramatically simply due to the varying sum of water dipoles being exerted on the surface. However, dipoles above the reaction plane generally do not affect the driving force for the reaction. We demonstrate this in Figure 7, which shows the electric field between the surface and the first water layer for two different water structures. We calculate the field between the metal and the first solvent bilayer as[40,70]

$$E_{\text{field}} = -\frac{dV_{\text{diff}}}{dz} \quad, \tag{21}$$

where the potential difference V_{diff} is defined as

$$V_{\text{diff}} = V_{\text{total}} - V_{\text{electrolyte}} - V_{\text{slab}} \quad. \tag{22}$$

Here V refers to the local electrostatic (ionic and Hartree) potential output by DFT. The subscript *total* refers to the local potential of the entire system, *electrolyte* refers to the local potential of just the electrolyte, and *slab* refers to the local potential of just the slab. This field reflects the local potential drop that would drive an electrochemical reaction or a chemical reaction involving polar adsorbates. In this picture, the first water layer is fixed while three water layers above have adopted different configurations that result in a nearly 4 eV shift in the work function. Further details regarding the generation of these data can be found in Note 4 in the SI. In summary, the reaction energetics are insensitive to the change in work function associated with the changing water dipoles above the reaction plane.
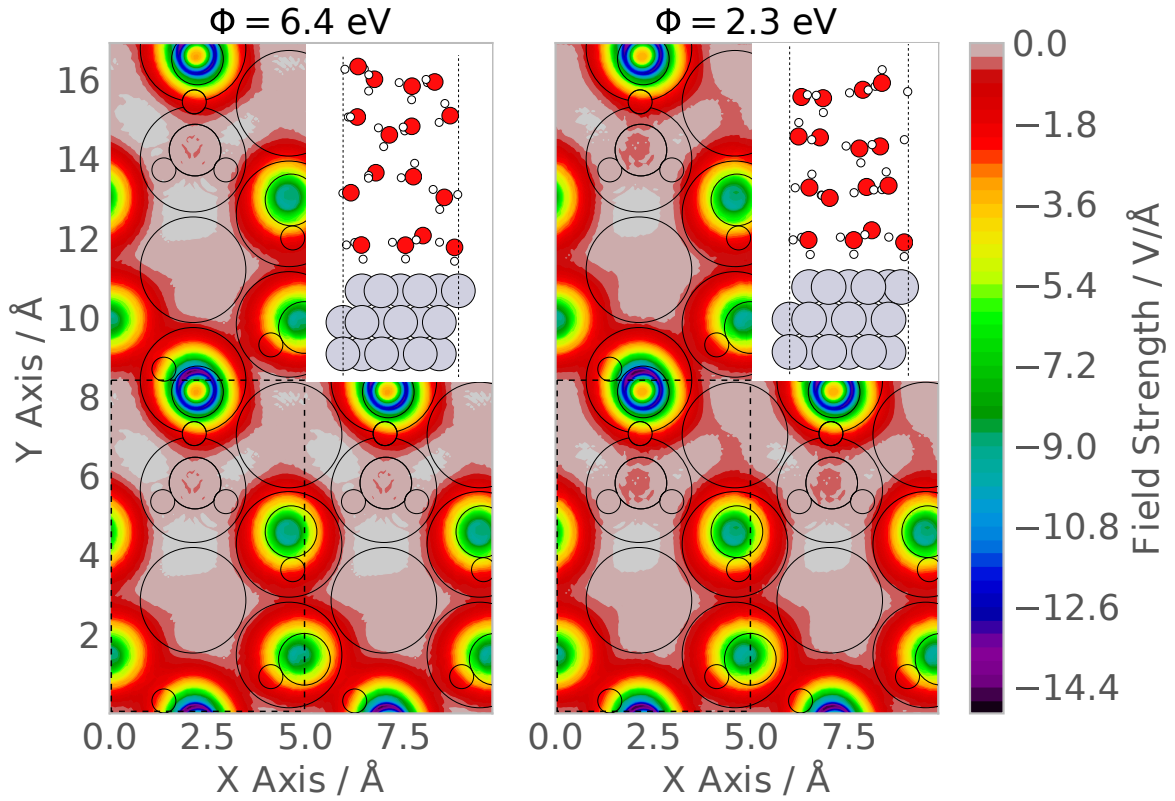
Figure 7: Electric field taken in a slice between the surface and the first water layer. Despite a nearly 4 eV difference in the work function between the left and right panels, the electric field at the interface is virtually identical, since the surface charge is roughly the same.

3.4 Insensitivity of the Driving Force to Continuum Charge Distribution

Another consequence of the effective surface charge density being the descriptor of driving force is the insensitivity of reaction energetics to the countercharge placement. In recent years, many different models of the electrolyte distribution have emerged, which have been shown to reproduce experimental capacitance curves at varying degrees of accuracy.[17,50–55,57–63,106] These charge placement models can have a significant effect on the simulated capacitance, which ranges from 13 to 18 $\mu F\,cm^{-2}$ (see SI Note 5), and potential of zero charge, and hence the predicted reaction energetics as a function of work function. However, as a function of surface charge, the energetics are largely insensitive. To demonstrate this idea, we have calculated the binding energy of two CO molecules on Cu (100) and Cu (211) using three countercharge placement models: planar countercharge, linear modified Poisson-Boltzmann, and modified Poisson-Boltzmann, as implemented in Environ.[47,107,107] Figure 8 illustrates that there is less than 10 meV variation in the reaction energetics as a function of surface charge for the two facets. Note that the abscissa in 8(a) contains just the continuum charge, and not that associated with adsorbed CO; the effective surface charge would include both contributions. However, because the charge due to CO is quite small, the effective surface charge is dominated by the continuum charging. Furthermore, including the small contribution of the CO dipole moment would result in a constant shift along the x-axis, resulting in the same conclusion.
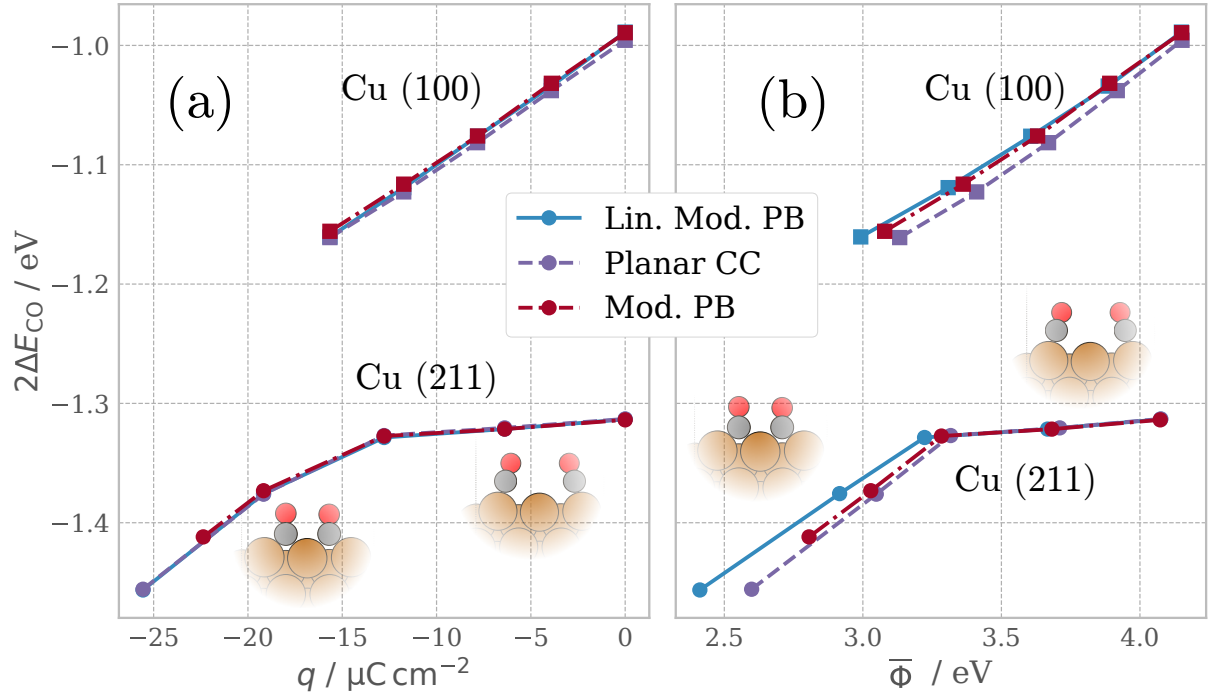
Figure 8: Illustration of the insensitivity of reaction energetics to the countercharge placement model. (a) Binding energy of two CO molecules on Cu (100) and Cu (211) as a function of surface charge for the three charge placement models. (b) Binding energy of two CO molecules on Cu (100) and Cu (211) as a function of work function. The nonlinear behavior observed for Cu (211) is due to a change in binding configuration as the surface charge is made more negative.

3.4.1 General Framework for Calculation of Electrochemical Reaction Energetics

To summarize, the models developed in this work can be applied to a general surface electrochemical reaction using a simple framework, illustrated in Figure 9.
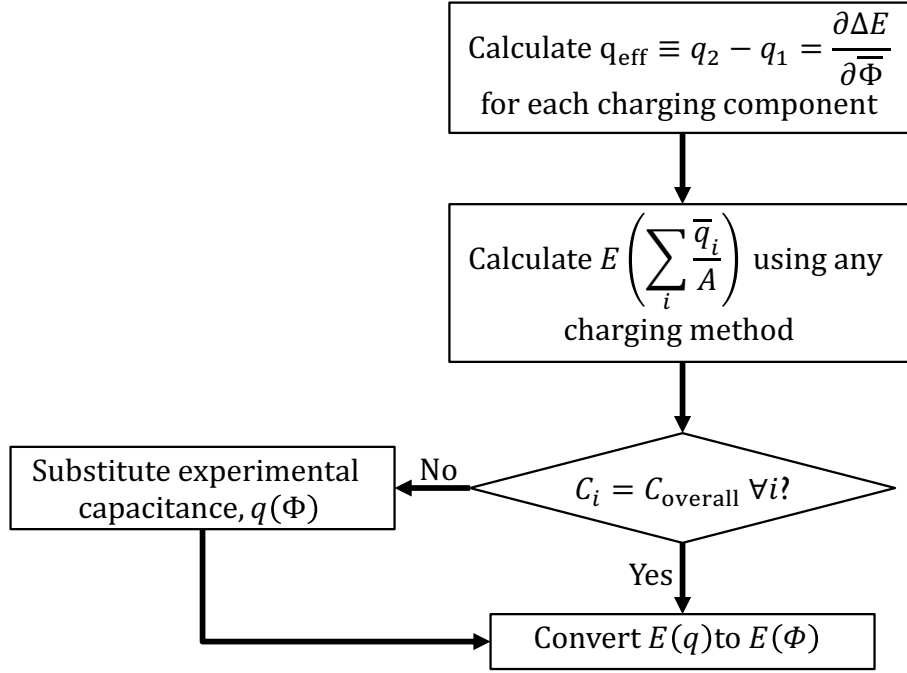

Figure 9: Flowchart illustrating the general framework for calculating electrochemical reaction energetics with the models presented in this work.

The first step, determining the effective charge q_{eff}, is performed by calculating the slope of the lines shown in Figure 5. Then, determining the energetics as a function of the effective surface charge is demonstrated to Figure 6 (b), where we show the Volmer reaction and CO_2 adsorption as a function of the total effective surface charge. The capacitance for each charging process (in the case of Figure 6 (b), explicit and implicit charging) can be calculated by, for instance, fitting $q = C(\Phi - \Phi_0)$, or equivalently, fitting Eq. 9. Among the two model reactions shown, only CO_2 adsorption satisfies the criteria that each capacitance is equivalent to the overall capacitance, and so the energetics as a function of charge can be directly converted to the energetics shown in Figure 6 (a). Here, the energetics are

uniquely determined by the potential. However, for the second case, the Volmer reaction (i.e. $(H^+ + e^-) + * \rightarrow H*$), it cannot be assumed that the two capacitances are equivalent to the overall capacitance, since they are quite different ($C_{\text{expl}} \approx 20 \mu\text{F cm}^{-2}$, $C_{\text{impl}} \approx 9 \mu\text{F cm}^{-2}$). Here, assuming an equivalent capacitance yields the energetics shown in Figure 6 (a), where it is clear that the energetics are not uniquely determined by the work function. Instead, the capacitance can be taken from an experimental charging curve for Pt (111), where it is found to have a capacitance of roughly $C \approx 20 \mu\text{F cm}^{-2}$.[108] For potentials far from the potential of zero charge, a more detailed charging function ($\Phi = f(q)$ for some f) could easily be substituted in lieu of the constant capacitance frequently reported in the literature (i.e. $\Phi = \frac{1}{C}q + \Phi_0$). With the energetics as a function of potential determined, they can then be input into a micro-kinetic model to determine, for instance, rates of electrochemical processes as a function of potential.

4   Conclusions

In this work, we have developed a general framework for the calculation of electrochemical reaction energetics from simulations of both explicit and implicit electrolyte. We demonstrate that the electrochemical interface can be effectively modeled as multiple capacitors, each corresponding to the separate charging components (i.e. separate dipole-field interactions). We show that an effective surface charge density, rather than the traditionally considered work function, is the appropriate descriptor for the driving force of electrochemical reactions. We illustrate this finding with the Volmer reaction and CO_2 adsorption. In the former the energetics are found to be multi-valued with respect to the work function. This framework allows us to, for the first time, effectively model the electrochemical interface using a hybrid explicit/continuum model in a way that is not dependent on cell size or predicted interfacial capacitance. These hybrid models are becoming increasingly popular as a way to treat the electrolyte in surface electrochemistry, since they allow for explicit treatment of charge in

27

charge transfer reactions, without the need for sampling of solvent states. They furthermore provide a simple way to probe large ranges of potential, without the need for costly extrapolation techniques. Future work will apply this method to reactions occurring in basic conditions, which previously was complicated by the aforementioned band misalignment challenges[68] with charged species at the interface, in addition to the usual challenges of sampling that occur with a purely explicit treatment of the electrolyte. Taken together, this work represents a significant advancement in the ability of modern computational tools to investigate surface electrochemical phenomena through the use of hybrid explicit/continuum solvation models coupled with DFT.

Acknowledgement

5 Supporting Information

The Supporting Information is available free of charge on the ACS Publications website. Further explanation of topics in the manuscript can be found in Notes 1-5 of the SI, along

with raw data to reproduce the figures found in the main text, including computational simulation input files.

References

(1) Schreiner, E.; Nair, N. N.; Wittekindt, C.; Marx, D. Peptide synthesis in aqueous environments: the role of extreme conditions and pyrite mineral surfaces on formation and hydrolysis of peptides. *J. Am. Chem. Soc.* **2011**, *133*, 8216–8226.

(2) Rimola, A.; Sodupe, M.; Ugliengo, P. Aluminosilicate surfaces as promoters for peptide bond formation: An assessment of Bernal's hypothesis by ab Initio methods. *J. Am. Chem. Soc.* **2007**, *129*, 8333–8344.

(3) Arrouvel, C.; Diawara, B.; Costa, D.; Marcus, P. DFT periodic study of the adsorption of glycine on the anhydrous and hydroxylated (0001) surfaces of α-alumina. *J. Phys. Chem. C* **2007**, *111*, 18164–18173.

(4) Irrera, S.; Costa, D.; Marcus, P. DFT periodic study of adsorption of glycine on the (0 0 0 1) surface of zinc terminated ZnO. *J. Mol. Struct.* **2009**, *903*, 49–58.

(5) Mignon, P.; Ugliengo, P.; Sodupe, M. Theoretical study of the adsorption of RNA/DNA bases on the external surfaces of Na+-montmorillonite. *J. Phys. Chem. C* **2009**, *113*, 13741–13749.

(6) Jiang, D.-e.; Cooper, V. R.; Dai, S. Porous graphene as the ultimate membrane for gas separation. *Nano Lett.* **2009**, *9*, 4019–4024.

(7) Hu, W.; Wu, X.; Li, Z.; Yang, J. Helium separation via porous silicene based ultimate membrane. *Nanoscale* **2013**, *5*, 9062–9066.

(8) Song, Q.; Nataraj, S.; Roussenova, M. V.; Tan, J. C.; Hughes, D. J.; Li, W.; Bourgoin, P.; Alam, M. A.; Cheetham, A. K.; Al-Muhtaseb, S. A.; Sivaniah, E. Zeolitic

imidazolate framework (ZIF-8) based polymer nanocomposite membranes for gas separation. *Energy Environ. Sci.* **2012**, *5*, 8359–8369.

(9) Kanai, Y.; Grossman, J. C. Role of semiconducting and metallic tubes in P3HT/carbon-nanotube photovoltaic heterojunctions: density functional theory calculations. *Nano Lett.* **2008**, *8*, 908–912.

(10) Appelhans, D. J.; Lin, Z.; Lusk, M. T. Two-dimensional carbon semiconductor: Density functional theory calculations. *Phys. Rev. B* **2010**, *82*, 073410.

(11) Ludwig, T.; Gauthier, J. A.; Brown, K. S.; Ringe, S.; Norskov, J. K.; Chan, K. Solvent-Adsorbate Interactions and Adsorbate-Specific Solvent Structure in Carbon Dioxide Reduction on a Stepped Cu Surface. *J. Phys. Chem. C* **2019**,

(12) Heenen, H. H.; Scheurer, C.; Reuter, K.; Voss, J.; Luntz, A. C. Multi-ion Conduction in Li3OCl Glass Electrolytes. *J. Phys. Chem. Lett.* **2019**,

(13) Dickens, C. F.; Nørskov, J. K. A Theoretical Investigation into the Role of Surface Defects for Oxygen Evolution on RuO2. *J. Phys. Chem. C* **2017**, *121*, 18516–18524.

(14) Liu, Z.-P.; Hu, P.; Alavi, A. Catalytic role of gold in gold-based catalysts: A density functional theory study on the CO oxidation on gold. *J. Am. Chem. Soc.* **2002**, *124*, 14770–14779.

(15) Yu, L.; Pan, X.; Cao, X.; Hu, P.; Bao, X. Oxygen reduction reaction mechanism on nitrogen-doped graphene: A density functional theory study. *J. Catal.* **2011**, *282*, 183–190.

(16) Wimmer, E.; Fu, C. L.; Freeman, A. J. Catalytic promotion and poisoning: All-electron local-density-functional theory of CO on Ni (001) surfaces coadsorbed with K or S. *Phys. Rev. Lett.* **1985**, *55*, 2618.

(17) Mamatkulov, M.; Filhol, J.-S. An ab initio study of electrochemical vs. electromechanical properties: the case of CO adsorbed on a Pt(111) surface. *Phys. Chem. Chem. Phys.* **2011**, *13*, 7675–7684.

(18) Katayama, Y.; Nattino, F.; Giordano, L.; Hwang, J.; Rao, R. R.; Andreussi, O.; Marzari, N.; Shao-Horn, Y. An In Situ Surface-Enhanced Infrared Absorption Spectroscopy Study of Electrochemical CO2 Reduction: Selectivity Dependence on Surface C-Bound and O-Bound Reaction Intermediates. *J. Phys. Chem. C* **2018**, *123*, 5951–5963.

(19) Heenen, H. H.; Scheurer, C.; Reuter, K. Implications of occupational disorder on ion mobility in Li4Ti5O12 battery materials. *Nano Lett.* **2017**, *17*, 3884–3888.

(20) Kortlever, R.; Shen, J.; Schouten, K. J. P.; Calle-Vallejo, F.; Koper, M. T. Catalysts and reaction pathways for the electrochemical reduction of carbon dioxide. *J. Phys. Chem. Lett.* **2015**, *6*, 4073–4082.

(21) Koper, M. T. Thermodynamic theory of multi-electron transfer reactions: Implications for electrocatalysis. *J. Electroanal. Chem.* **2011**, *660*, 254–260.

(22) Calle-Vallejo, F.; Koper, M. T. Theoretical considerations on the electroreduction of CO to C2 species on Cu (100) electrodes. *Angew. Chem.* **2013**, *52*, 7282–7285.

(23) Nørskov, J. K.; Rossmeisl, J.; Logadottir, A.; Lindqvist, L.; Kitchin, J. R.; Bligaard, T.; Jonsson, H. Origin of the overpotential for oxygen reduction at a fuel-cell cathode. *J. Phys. Chem. B* **2004**, *108*, 17886–17892.

(24) Liu, X.; Xiao, J.; Peng, H.; Hong, X.; Chan, K.; Nørskov, J. K. Understanding trends in electrochemical carbon dioxide reduction rates. *Nat. Commun.* **2017**, *8*, 15438.

(25) Tripković, V.; Skúlason, E.; Siahrostami, S.; Nørskov, J. K.; Rossmeisl, J. The oxygen

reduction reaction mechanism on Pt (1 1 1) from density functional theory calculations. *Electrochim. Acta* **2010**, *55*, 7975–7981.

(26) Nie, X.; Luo, W.; Janik, M. J.; Asthagiri, A. Reaction mechanisms of CO2 electrochemical reduction on Cu (1 1 1) determined with density functional theory. *J. Catal.* **2014**, *312*, 108–122.

(27) Hyman, M. P.; Medlin, J. W. Mechanistic study of the electrochemical oxygen reduction reaction on Pt (111) using density functional theory. *J. Phys. Chem. B* **2006**, *110*, 15338–15344.

(28) Vassilev, P.; Koper, M. T. Electrochemical reduction of oxygen on gold surfaces: a density functional theory study of intermediates and reaction paths. *J. Phys. Chem. C* **2007**, *111*, 2607–2613.

(29) Skúlason, E.; Tripkovic, V.; Bjorketun, M. E.; Gudmundsdottir, S.; Karlberg, G.; Rossmeisl, J.; Bligaard, T.; Jónsson, H.; Nørskov, J. K. Modeling the electrochemical hydrogen oxidation and evolution reactions on the basis of density functional theory calculations. *J. Phys. Chem. C* **2010**, *114*, 18182–18197.

(30) Skúlason, E.; Karlberg, G. S.; Rossmeisl, J.; Bligaard, T.; Greeley, J.; Jónsson, H.; Nørskov, J. K. Density functional theory calculations for the hydrogen evolution reaction in an electrochemical double layer on the Pt (111) electrode. *Phys. Chem. Chem. Phys.* **2007**, *9*, 3241–3250.

(31) Zhang, J.; Wang, Z.; Zhu, Z. The inherent kinetic electrochemical reduction of oxygen into H2O on FeN4-carbon: a density functional theory study. *J. Power Sources* **2014**, *255*, 65–69.

(32) Yeh, K.-Y.; Janik, M. J. Density functional theory-based electrochemical models for the oxygen reduction reaction: Comparison of modeling approaches for electric field and solvent effects. *J. Comput. Chem.* **2011**, *32*, 3399–3408.

(33) Shi, C.; Chan, K.; Yoo, J. S.; Nørskov, J. K. Barriers of electrochemical CO2 reduction on transition metals. *Org. Process Res. Dev.* **2016**, *20*, 1424–1430.

(34) Lessio, M.; Senftle, T. P.; Carter, E. A. Hydride Shuttle Formation and Reaction with CO2 on GaP (110). *ChemSusChem* **2018**, *11*, 1558–1566.

(35) Liao, P.; Keith, J. A.; Carter, E. A. Water oxidation on pure and doped hematite (0001) surfaces: Prediction of Co and Ni as effective dopants for electrocatalysis. *J. Am. Chem. Soc.* **2012**, *134*, 13296–13309.

(36) Sakong, S.; Groß, A. The importance of the electrochemical environment in the electro-oxidation of methanol on Pt (111). *ACS Catal.* **2016**, *6*, 5575–5586.

(37) Stecher, T.; Reuter, K.; Oberhofer, H. First-Principles Free-Energy Barriers for Photoelectrochemical Surface Reactions: Proton Abstraction at TiO 2 (110). *Phys. Rev. Lett.* **2016**, *117*, 276001.

(38) Montoya, J. H.; Shi, C.; Chan, K.; Nørskov, J. K. Theoretical insights into a CO dimerization mechanism in CO2 electroreduction. *J. Phys. Chem. Lett.* **2015**, *6*, 2032–2037.

(39) Karlberg, G.; Rossmeisl, J.; Nørskov, J. K. Estimations of electric field effects on the oxygen reduction reaction based on the density functional theory. *Phys. Chem. Chem. Phys.* **2007**, *9*, 5158–5161.

(40) Chen, L. D.; Urushihara, M.; Chan, K.; Nørskov, J. K. Electric field effects in electrochemical CO2 reduction. *ACS Catal.* **2016**, *6*, 7133–7139.

(41) Strmcnik, D.; Uchimura, M.; Wang, C.; Subbaraman, R.; Danilovic, N.; Van Der Vliet, D.; Paulikas, A. P.; Stamenkovic, V. R.; Markovic, N. M. Improving the hydrogen oxidation reaction rate by promotion of hydroxyl adsorption. *Nat. Chem.* **2013**, *5*, 300.

(42) Liu, X.; Schlexer, P.; Xiao, J.; Ji, Y.; Wang, L.; Sandberg, R. B.; Tang, M.; Brown, K. S.; Peng, H.; Ringe, S.; Hahn, C.; Jaramillo, T. F.; Nørskov, J. K.; Chan, K. pH effects on the electrochemical reduction of CO (2) towards C 2 products on stepped copper. *Nat. Commun.* **2019**, *10*, 32.

(43) Rossmeisl, J.; Chan, K.; Ahmed, R.; Tripković, V.; Björketun, M. E. pH in atomic scale simulations of electrochemical interfaces. *Phys. Chem. Chem. Phys.* **2013**, *15*, 10321–10325.

(44) Rossmeisl, J.; Skúlason, E.; Björketun, M. E.; Tripkovic, V.; Nørskov, J. K. Modeling the electrified solid–liquid interface. *Chem. Phys. Lett.* **2008**, *466*, 68–71.

(45) Chan, K.; Nørskov, J. K. Potential dependence of electrochemical barriers from ab initio calculations. *J. Phys. Chem. Lett.* **2016**, *7*, 1686–1690.

(46) Chan, K.; Nørskov, J. K. Electrochemical barriers made simple. *J. Phys. Chem. Lett.* **2015**, *6*, 2663–2668.

(47) Andreussi, O.; Dabo, I.; Marzari, N. Revised self-consistent continuum solvation in electronic-structure calculations. *J. Chem. Phys.* **2012**, *136*, 064102.

(48) Kastlunger, G.; Lindgren, P.; Peterson, A. A. Controlled-potential simulation of elementary electrochemical reactions: Proton discharge on metal surfaces. *J. Phys. Chem. C* **2018**, *122*, 12771–12781.

(49) Otani, M.; Sugino, O. First-principles calculations of charged surfaces and interfaces: A plane-wave nonrepeated slab approach. *Phys. Rev. B* **2006**, *73*, 115407.

(50) Lozovoi, A.; Alavi, A.; Kohanoff, J.; Lynden-Bell, R. Ab initio simulation of charged slabs at constant chemical potential. *J. Chem. Phys.* **2001**, *115*, 1661–1669.

(51) Taylor, C. D.; Wasileski, S. A.; Filhol, J.-S.; Neurock, M. First principles reaction

modeling of the electrochemical interface: Consideration and calculation of a tunable surface potential from atomic and electronic structure. *Phys. Rev. B* **2006**, *73*, 165402.

(52) Fang, Y.-H.; Liu, Z.-P. Surface phase diagram and oxygen coupling kinetics on flat and stepped Pt surfaces under electrochemical potentials. *J. Phys. Chem. C* **2009**, *113*, 9765–9772.

(53) Fang, Y.-H.; Liu, Z.-P. Mechanism and tafel lines of electro-oxidation of water to oxygen on RuO2 (110). *J. Am. Chem. Soc.* **2010**, *132*, 18214–18222.

(54) Ringe, S.; Oberhofer, H.; Hille, C.; Matera, S.; Reuter, K. Function-space-based solution scheme for the size-modified Poisson–Boltzmann equation in full-potential DFT. *J. Chem. Theory Comput.* **2016**, *12*, 4052–4066.

(55) Jinnouchi, R.; Anderson, A. B. Aqueous and surface redox potentials from self-consistently determined gibbs energies. *J. Phys. Chem. C* **2008**, *112*, 8747–8750.

(56) Mathew, K.; Sundararaman, R.; Letchworth-Weaver, K.; Arias, T.; Hennig, R. G. Implicit solvation model for density-functional study of nanocrystal surfaces and reaction pathways. *J. Chem. Phys.* **2014**, *140*, 084106.

(57) Mathew, K.; Hennig, R. G. Implicit self-consistent description of electrolyte in plane-wave density-functional theory. *arXiv preprint arXiv:1601.03346* **2016**,

(58) Fisicaro, G.; Genovese, L.; Andreussi, O.; Marzari, N.; Goedecker, S. A generalized Poisson and Poisson-Boltzmann solver for electrostatic environments. *J. Chem. Phys.* **2016**, *144*, 014103.

(59) Fang, Y.-H.; Wei, G.-F.; Liu, Z.-P. Theoretical modeling of electrode/electrolyte interface from first-principles periodic continuum solvation method. *Catal. Today* **2013**, *202*, 98–104.

(60) Letchworth-Weaver, K.; Arias, T. Joint density functional theory of the electrode-electrolyte interface: Application to fixed electrode potentials, interfacial capacitances, and potentials of zero charge. *Phys. Rev. B* **2012**, *86*, 075140.

(61) Keilbart, N.; Okada, Y.; Feehan, A.; Higai, S.; Dabo, I. Quantum-continuum simulation of the electrochemical response of pseudocapacitor electrodes under realistic conditions. *Phys. Rev. B* **2017**, *95*, 115423.

(62) Sundararaman, R.; Schwarz, K. Evaluating continuum solvation models for the electrode-electrolyte interface: Challenges and strategies for improvement. *J. Chem. Phys.* **2017**, *146*, 084111.

(63) Minezawa, N.; Kato, S. Efficient implementation of three-dimensional reference interaction site model self-consistent-field method: Application to solvatochromic shift calculations. *J. Chem. Phys.* **2007**, *126*, 054511.

(64) Nattino, F.; Truscott, M.; Marzari, N.; Andreussi, O. Continuum models of the electrochemical diffuse layer in electronic-structure calculations. *J. Chem. Phys.* **2019**, *150*, 041722.

(65) Gauthier, J.; Dickens, C. F.; Chen, L. D.; Doyle, A. D.; Norskov, J. K. Solvation Effects for Oxygen Evolution Reaction Catalysis on IrO_2 (110). *J. Phys. Chem. C* **2017**, *2*.

(66) Kristoffersen, H. H.; Vegge, T.; Hansen, H. A. OH formation and H 2 adsorption at the liquid water–Pt (111) interface. *Chem. Sci.* **2018**, *9*, 6912–6921.

(67) Sakong, S.; Groß, A. The electric double layer at metal-water interfaces revisited based on a charge polarization scheme. *J. Chem. Phys.* **2018**, *149*, 084705.

(68) Björketun, M. E.; Zeng, Z.; Ahmed, R.; Tripkovic, V.; Thygesen, K. S.; Rossmeisl, J.

Avoiding pitfalls in the modeling of electrochemical interfaces. *Chem. Phys. Lett.* **2013**, *555*, 145–148.

(69) Perdew, J. P. Density functional theory and the band gap problem. *Int. J. Quantum Chem.* **1985**, *28*, 497–523.

(70) Gauthier, J. A.; Ringe, S.; Dickens, C. F.; Garza, A. J.; Bell, A. T.; Head-Gordon, M.; Nørskov, J. K.; Chan, K. Challenges in Modeling Electrochemical Reaction Energetics with Polarizable Continuum Models. *ACS Catal.* **2018**, *9*, 920–931.

(71) Ringe, S.; Oberhofer, H.; Reuter, K. Transferable ionic parameters for first-principles Poisson-Boltzmann solvation calculations: Neutral solutes in aqueous monovalent salt solutions. *J. Chem. Phys.* **2017**, *146*, 134103.

(72) Karlberg, G. Adsorption trends for water, hydroxyl, oxygen, and hydrogen on transition-metal and platinum-skin surfaces. *Phys. Rev. B* **2006**, *74*, 153414.

(73) Rossmeisl, J.; Greeley, J.; Karlberg, G. Electrocatalysis and catalyst screening from density functional theory calculations. *Fuel Cell Catalysis: A Surface Science Approach* **2009**, 57–92.

(74) Briquet, L. G.; Sarwar, M.; Mugo, J.; Jones, G.; Calle-Vallejo, F. A new type of scaling relations to assess the accuracy of computational predictions of catalytic activities applied to the oxygen evolution reaction. *ChemCatChem* **2017**, *9*, 1261–1268.

(75) Goodpaster, J. D.; Bell, A. T.; Head-Gordon, M. Identification of possible pathways for C–C bond formation during electrochemical reduction of CO2: New theoretical insights from an improved electrochemical model. *J. Phys. Chem. Lett.* **2016**, *7*, 1471–1477.

(76) Saleheen, M.; Heyden, A. Liquid Phase Modeling in Heterogeneous Catalysis. *ACS Catal.* **2018**,

(77) Jensen, F. *Introduction of Computational Chemistry*, 2nd ed.; John Wiley & Sons: Chichester, 2007.

(78) Tang, W.; Sanville, E.; Henkelman, G. A grid-based Bader analysis algorithm without lattice bias. *J. Phys. Condens. Matter* **2009**, *21*, 084204.

(79) Sanville, E.; Kenny, S. D.; Smith, R.; Henkelman, G. Improved grid-based algorithm for Bader charge allocation. *J. Comput. Chem.* **2007**, *28*, 899–908.

(80) Henkelman, G.; Arnaldsson, A.; Jónsson, H. A fast and robust algorithm for Bader decomposition of charge density. *Comput. Mater. Sci.* **2006**, *36*, 354–360.

(81) Frumkin, A. Wasserstoffüberspannung und Struktur der Doppelschicht. *Zeitschrift für physikalische Chemie* **1933**, *164*, 121–133.

(82) Van Soestbergen, M. Frumkin-Butler-Volmer theory and mass transfer in electrochemical cells. *Russ. J. Electrochem.* **2012**, *48*, 570–579.

(83) Ringe, S.; Clark, E. L.; Resasco, J.; Walton, A.; Seger, B. J.; Bell, A. T.; Chan, K. Understanding Cation Effects in Electrochemical CO_2 Reduction. *Energy Environ. Sci.* **2019**,

(84) Kresse, G.; Hafner, J. Ab initio molecular dynamics for liquid metals. *Phys. Rev. B* **1993**, *47*, 558–561.

(85) Kresse, G.; Furthmüller, J. Efficient iterative schemes for ab initio total-energy calculations using a plane-wave basis set. *Phys. Rev. B* **1996**, *54*, 11169–11186.

(86) Kresse, G.; Furthmüller, J. Efficiency of ab-initio total energy calculations for metals and semiconductors using a plane-wave basis set. *Comput. Mater. Sci.* **1996**, *6*, 15–50.

(87) Giannozzi, P.; Baroni, S.; Bonini, N.; Calandra, M.; Car, R.; Cavazzoni, C.; Ceresoli, D.; Chiarotti, G. L.; Cococcioni, M.; Dabo, I.; Corso, A. D.; de Gironcoli, S.;

Fabris, S.; Fratesi, G.; Gebauer, R.; Gerstmann, U.; Gougoussis, C.; Kokalj, A.; Lazzeri, M.; Martin-Samos, L.; Marzari, N.; Mauri, F.; Mazzarello, R.; Paolini, S.; Pasquarello, A.; Paulatto, L.; Sbraccia, C.; Scandolo, S.; Sclauzero, G.; Seitsonen, A. P.; Smogunov, A.; Umari, P.; Wentzcovitch, R. M. QUANTUM ESPRESSO: A Modular and Open-Source Software Project for Quantum Simulations of Materials. *J. Phys. Condens. Matter* **2009**, *21*, 395502.

(88) Garrity, K. F.; Bennett, J. W.; Rabe, K. M.; Vanderbilt, D. Pseudopotentials for high-throughput DFT calculations. *Comput. Mater. Sci.* **2014**, *81*, 446–452.

(89) Hammer, B.; Hansen, L. B.; Nørskov, J. K. Improved adsorption energetics within density-functional theory using revised Perdew-Burke-Ernzerhof functionals. *Phys. Rev. B* **1999**, *59*, 7413.

(90) Monkhorst, H. J.; Pack, J. D. Special points for Brillouin-zone integrations. *Phys. Rev. B* **1976**, *13*, 5188.

(91) Gauthier, J. A.; Dickens, C. F.; Ringe, S.; Chan, K. Practical Considerations for Continuum Models Applied to Surface Electrochemistry. *ChemPhysChem* **2019**,

(92) Chen, L. D.; Bajdich, M.; Martirez, J. M. P.; Krauter, C. M.; Gauthier, J. A.; Carter, E. A.; Luntz, A. C.; Chan, K.; Nørskov, J. K. Understanding the apparent fractional charge of protons in the aqueous electrochemical double layer. *Nat. Commun.* **2018**, *9*, 3202.

(93) de Levie, R. The electrosorption valency and partial charge transfer. *J. Electroanal. Chem.* **2004**, *562*, 273–276.

(94) Grahame, D. C. Components of charge and potential in the non-diffuse region of the electrical double layer: potassium iodide solutions in contact with mercury at 25. *J. Am. Chem. Soc.* **1958**, *80*, 4201–4210.

(95) Schultze, J.; Rolle, D. The partial discharge of electrosorbates and its influence in electrocatalysis. *Can. J. Chem. journal of chemistry* **1997**, *75*, 1750–1758.

(96) Dabo, I.; Li, Y.; Bonnet, N.; Marzari, N. Ab initio electrochemical properties of electrode surfaces. *Fuel Cell Science: Theory, Fundamentals, and Biocatalysis* **2010**, 415–431.

(97) Bonnet, N.; Dabo, I.; Marzari, N. Chemisorbed molecules under potential bias: detailed insights from first-principles vibrational spectroscopies. *Electrochim. Acta* **2014**, *121*, 210–214.

(98) Filhol, J.-S.; Doublet, M.-L. An ab initio study of surface electrochemical disproportionation: The case of a water monolayer adsorbed on a Pd (1 1 1) surface. *Catal. Today* **2013**, *202*, 87–97.

(99) Steinmann, S. N.; Michel, C.; Schwiedernoch, R.; Sautet, P. Impacts of electrode potentials and solvents on the electroreduction of CO 2: a comparison of theoretical approaches. *Phys. Chem. Chem. Phys.* **2015**, *17*, 13949–13963.

(100) Sundararaman, R.; Letchworth-Weaver, K.; Schwarz, K. A. Improving accuracy of electrochemical capacitance and solvation energetics in first-principles calculations. *J. Chem. Phys.* **2018**, *148*, 144105.

(101) Merlet, C.; Limmer, D. T.; Salanne, M.; Van Roij, R.; Madden, P. A.; Chandler, D.; Rotenberg, B. The electric double layer has a life of its own. *J. Phys. Chem. C* **2014**, *118*, 18291–18298.

(102) Limmer, D. T. Interfacial ordering and accompanying divergent capacitance at ionic liquid-metal interfaces. *Phys. Rev. Lett.* **2015**, *115*, 256102.

(103) Van den Bossche, M.; Skúlason, E.; Rose-Petruck, C.; Jónsson, H. Assessment of

Constant-Potential Implicit Solvation Calculations of Electrochemical Energy Barriers for H2 Evolution on Pt. *J. Phys. Chem. C* **2019**,

(104) Steinmann, S. N.; Sautet, P. Assessing a first-principles model of an electrochemical interface by comparison with experiment. *J. Phys. Chem. C* **2016**, *120*, 5619–5623.

(105) Sundararaman, R.; Letchworth-Weaver, K.; Schwarz, K. A.; Gunceler, D.; Ozhabes, Y.; Arias, T. JDFTx: software for joint density-functional theory. *SoftwareX* **2017**, *6*, 278–284.

(106) Borukhov, I.; Andelman, D.; Orland, H. Adsorption of large ions from an electrolyte solution: a modified Poisson–Boltzmann equation. *Electrochim. Acta* **2000**, *46*, 221–229.

(107) Andreussi, O.; Hormann, N. G.; Nattino, F.; Fisicaro, G.; Goedecker, S.; Marzari, N. Solvent-aware interfaces in continuum solvation. *J. Chem. Theory Comput.* **2019**,

(108) Pajkossy, T.; Kolb, D. M. Double layer capacitance of Pt (111) single crystal electrodes. *Electrochim. Acta* **2001**, *46*, 3063–3071.

Graphical TOC Entry